

High Breakdown Electric Field (> 5 MV/cm) in UWBG AlGa_N Transistors

Seunghoon Shin^{1,a)}, Hridibrata Pal³, Jon Pratt¹, John Niroula³, Yinxuan Zhu¹, Chandan Joishi¹, Brianna A. Klein⁴, Andrew Armstrong⁴, Andrew A. Allerman⁴, Tomás Palacios³, Siddharth Rajan^{1,2,a)}

¹*Department of Electrical & Computer Engineering, The Ohio State University, Columbus OH 43210, USA*

²*Department of Materials Science & Engineering, The Ohio State University, Columbus OH 43210*

³*Microsystems Technology Laboratories, Massachusetts Institute of Technology, Cambridge, Massachusetts 02139, USA*

⁴*Sandia National Laboratories, Albuquerque, New Mexico 87123, USA*

Abstract:

We report on the design and demonstration of ultra-wide bandgap (UWBG) AlGa_N-channel metal-insulator heterostructure field effect transistors (HEFTs) for high-power, high-frequency applications. We find that the integration of gate dielectrics and field plates greatly improves the breakdown field in these devices, with state-of-art average breakdown field of 5.3 MV/cm (breakdown voltage > 260 V) with an associated maximum current density of 342 mA/mm, and cut-off frequency of 9.1 GHz. Furthermore, low trap-related impact was observed from minimal gate and drain lag estimated from pulsed I-V characteristics. The reported results provide the potential of UWBG AlGa_N HEFTs for the next generation high-power radio frequency applications.

^{a)} Authors to whom correspondence should be addressed

Electronic mail: shin.928@osu.edu, rajan.21@osu.edu

Ultra-wide bandgap (UWBG) AlGa_N is a promising candidate material for future RF and mm-wave applications due to its high breakdown field and excellent transport properties. The Johnson figure of merit (JFOM)—a key figure of merit to estimate the product of the cut-off frequency (f_T) and breakdown voltage (V_{BR})—is expected to be 22 THz·V [1], which is significantly higher than that of state-of-art GaN or InP devices. However, high contact resistance remains a practical limitation to AlGa_N transistors. To improve ohmic contact properties, recent work by Zhu et al. achieved a state-of-art R_C of 0.25 $\Omega\cdot\text{mm}$ to n-type AlGa_N by incorporating reverse-graded contacts and bandgap narrowing effect in UWBG AlGa_N [7], while approaches such as advanced regrowth techniques have also shown encouraging results [14, 33, 34]. Several demonstrations of UWBG AlGa_N heterostructure field effect transistors (HEFTs) over the last decade have shown consistent improvement [9]. However, the reported average breakdown fields (F_{BR}) in AlGa_N transistors have been relatively low, typically below 3.6 MV/cm. [16]. In this study, we report on the successful demonstration of UWBG AlGa_N metal-insulator HFETs with breakdown fields in excess >of 5 MV/cm.

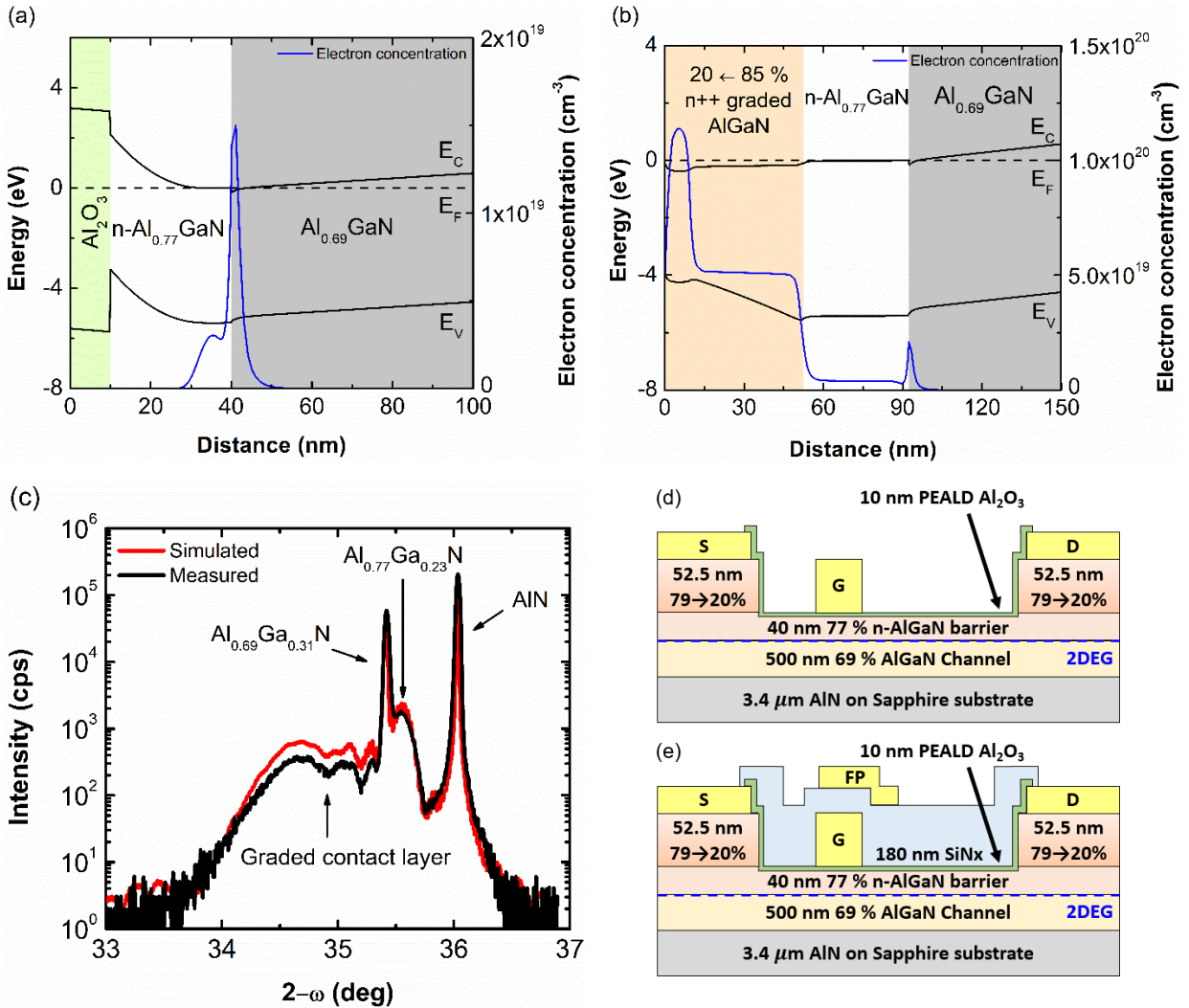


Figure 1. Calculated equilibrium energy band diagram (a) under the gate, (b) under the ohmic contact region, (c) XRD 2 θ - ω scan of epitaxial stack, Schematic of device structures (d) Sample B, (e) Sample C

The epitaxial layers used for device fabrication were grown on a TNSC-4000HT metal-organic chemical vapor deposition (MOCVD) reactor on previously grown AlN/Sapphire templates. The epitaxial stack consists of 500 nm 69% Al-content AlGa_N channel, a 40 nm thick 77 % n-AlGa_N barrier (Si = 4×10^{18} cm⁻³), and reverse-graded contact layers (Al% \sim 79 % to 20 %) [7]. The 40 nm-thick barrier was designed to enable over-etching into the barrier, ensuring the complete removal of the contact layer in the access region after etching, while also preventing ICP-RIE-induced damage. The AlGa_N layer Al compositions and thicknesses were confirmed with high-resolution x-ray diffraction (HR-XRD) measurements on a Bruker D8 Discover system. As shown in Figure 1(c), the measured and simulated XRD spectra show good match.

Figure 1(a), (b) presents the equilibrium energy band diagram for gate (Figure. 1(a)) and ohmic region (Figure 1(b)), which were built based on the XRD results. The barrier height between Ni/Al₂O₃ was assumed as 3.2 eV [35-36]. From the simulated energy band diagram, the expected total charge density and two-dimensional electron charge density ($n_{2\text{DEG}}$) were 7.16×10^{12} cm⁻² and 4.72×10^{12} cm⁻², respectively.

Table 1. Device Dimensions

	L_{SG} (μm)	L_G (μm)	L_{GD} (μm)	t_{ox}	Passivation	L_{FP} (μm)
Sample A	0.5	0.8	0.7	-	-	-
Sample B	0.5	1	0.5	10 nm Al ₂ O ₃	-	-
Sample C	0.5	1	0.5	10 nm Al ₂ O ₃	180 nm SiN _x	0.25

Direct-write optical lithography was used for patterning of all deposition and etch steps described below. The contact layer was etched using a low-damage ICP-RIE process (BCl₃/Cl₂/Ar = 5/50/5 sccm, ICP/RIE power = 40/8 W at 5 mTorr) into the 77 % barrier layer. The estimated barrier thickness after etching was estimated to be 29.5 nm using atomic force microscopy. Ti/Al/Ni/Au (20/120/30/100 nm) ohmic metal was patterned using electron-beam evaporation and lift-off in NMP. A 10 nm PEALD Al₂O₃ was deposited at 250 °C using TMA and O₂ as precursors with a growth rate of 1 Å/cycle. Mesa isolation was done using ICP-RIE etching (etch depth of 200 nm) and Ni/Au/Ni (30/100/50 nm) gate layers were deposited using e-beam evaporation and lift-off. Plasma-enhanced chemical vapor deposition (PECVD) SiN_x (180 nm) was deposited as a passivation layer, and Ni/Au gate-connected field plates were evaporated. The electrical characteristics of three samples (Table 1) are outlined in this paper: (1) Sample A, field effect transistors fabricated without Al₂O₃ gate dielectric SiN_x, (2) Sample B, transistors with Al₂O₃ gate dielectric but with no field plate, and (3) and Sample C, transistors with Al₂O₃ gate dielectric, SiN_x passivation and a field plate (Figure 1(b)-(c)).

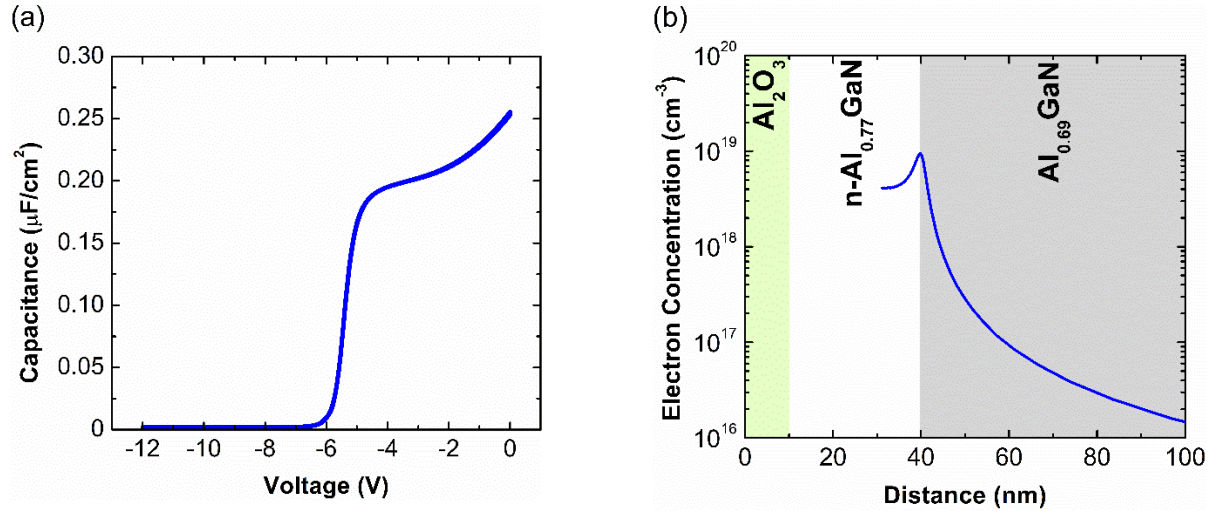


Figure 2. (a) Double-sweep C-V results after Al_2O_3 integration, (b) extracted electron concentration profile corresponding to gate sweep from 0 V to -12 V.

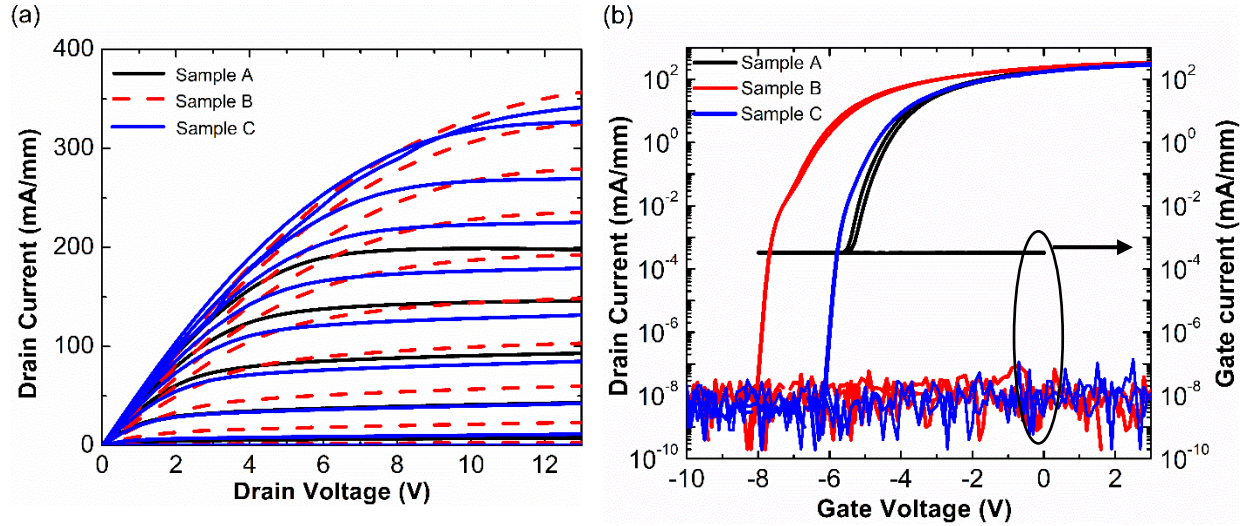


Figure 3. (a) Output curves with DC bias condition of $\Delta V_{\text{GS}} = -1$ V, $V_{\text{GS}} = 0 \sim -5$ V for Sample A, $\Delta V_{\text{GS}} = -1$ V, $V_{\text{GS}} = 3 \sim -6$ V for Sample B and C, (b) transfer curves at $V_{\text{DS}} = 10$ V for different device structures

The sheet resistance, Hall carrier density, and Hall mobility for the channel regions (with the contact layer etched away) were estimated to be $6.79 \text{ k}\Omega/\square$, $6 \times 10^{12} \text{ cm}^{-2}$, and $153 \text{ cm}^2/\text{V}\cdot\text{s}$, respectively. A contact resistance of $3.26 \text{ }\Omega\cdot\text{mm}$ and specific contact resistivity of $1.86 \times 10^{-5} \text{ }\Omega\cdot\text{cm}^2$ were estimated from transmission line measurements (TLM). The contact resistance is higher than that seen for reverse-graded contacts made directly to n-type AlGaIn [7]. We attribute this to the additional conduction band barrier introduced by the heterojunction. Capacitance-voltage (C-V) and DC I-V characteristics were

measured using a Keysight B1500A. C-V measurements on metal-Al₂O₃-AlGaIn capacitors showed hysteresis-free behavior under double-sweep voltage measurements (Figure 2(a)), and the integrated sheet charge density from pinch-off to zero bias was estimated to be $7.15 \times 10^{12} \text{ cm}^{-2}$ (Figure 2(b)). The charge profile extracted from C-V measurements suggests apparent charge density ($\sim 4 \times 10^{18} \text{ cm}^{-3}$) in the barrier layer, and a 2-dimensional electron gas as expected at the heterojunction, at a depth of 39.5 nm. Integration of the charge profile shows that the majority of the charge ($4.6 \times 10^{12} \text{ cm}^{-2}$) is contained in the 2-dimensional electron gas.

Sample B showed threshold voltage (V_{TH}) of -8 V and maximum on-current (I_{MAX}) of 358 mA/mm at $V_{\text{GS}} = +3 \text{ V}$ (Figure 3(a)), while Sample C exhibited $V_{\text{TH}} = -7 \text{ V}$, and $I_{\text{MAX}} = 342 \text{ mA/mm}$ at $V_{\text{GS}} = 3 \text{ V}$ and. We attribute the relatively minor V_{TH} variation between samples to differences in the epitaxial layer structure. At $V_{\text{DS}} = 10 \text{ V}$ the maximum transconductance ($g_{\text{m,MAX}}$) for Sample A was 48 mS/mm and that for Sample B was 49 mS/mm. The gate leakage current for the baseline HFET was relatively high without the Al₂O₃ gate dielectric, resulting in $I_{\text{ON}}/I_{\text{OFF}}$ ratio ($< 6 \times 10^5$) (Figure 3(b)). However, integration of 10 nm Al₂O₃ significantly reduced the gate leakage current to sub nA/mm levels, enhancing the $I_{\text{ON}}/I_{\text{OFF}}$ ratio to 2×10^{10} .

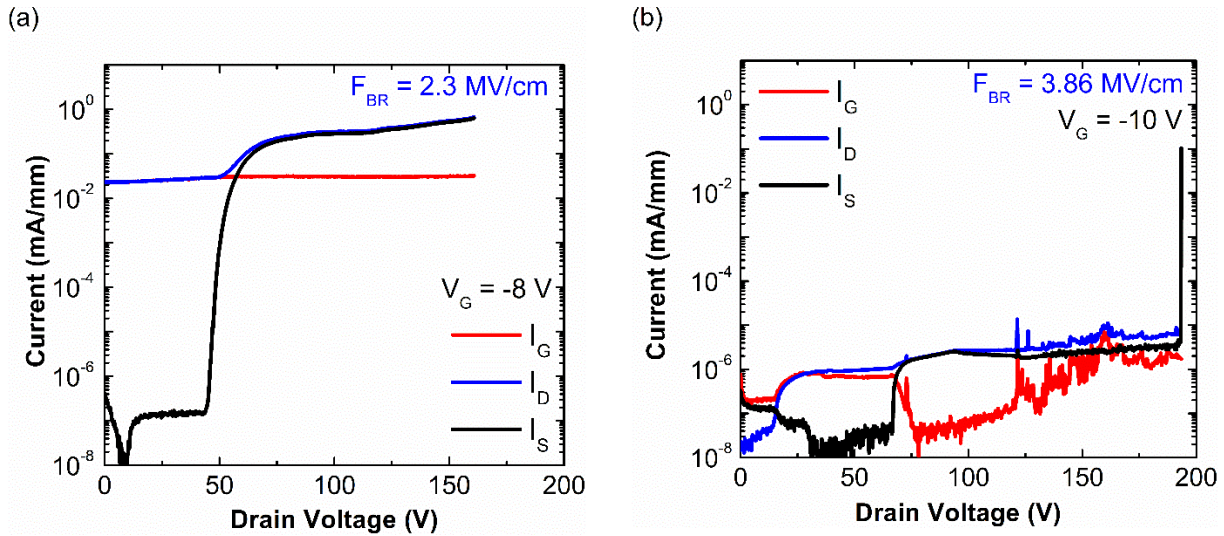


Figure 4. Three-terminal currents as a function of drain bias for (a) Sample A, and (b) Sample B

Three-terminal off-state leakage currents were measured using Keysight B1500A within the 200 V DC bias range while higher voltage characteristics were investigated using a Keysight B1505A power device analyzer. Without Al₂O₃ gate dielectric, relatively high gate leakage was observed, possibly due to the high doping concentration in the AlGaIn barrier layer (Figure 4(a)), but the leakage current reduces after deposition of Al₂O₃, as shown in Figure 4(b). For Sample B, the gate leakage remained below $1 \times 10^{-5} \text{ mA/mm}$ at $V_{\text{GS}} = -10 \text{ V}$ and $V_{\text{DS}} = 193 \text{ V}$ (Figure 4(b)). This result is consistent with previous work on

PEALD $\text{Al}_2\text{O}_3/\text{AlGaIn}$ structures, and shows that the dielectric effectively reduces and suppresses gate leakage current [10].

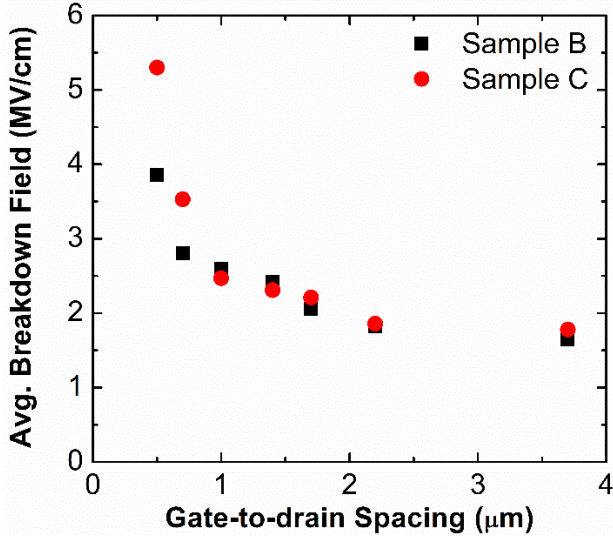


Figure 5. Average maximum breakdown field (F_{BR}) as a function of the gate-drain spacing (L_{GD}) transistors with gate dielectric/no passivation (Sample B), and with gate dielectric + passivation + field plate (Sample C)

The L_{GD} -dependent relationship between F_{BR} and breakdown voltage was investigated by measuring the breakdown voltage while varying the gate-to-drain spacing. By plotting F_{BR} as a function of L_{GD} , it was observed that F_{BR} decreases with increasing L_{GD} (Figure 5). The breakdown voltage for the purpose of this paper was defined as the voltage where the current reaches 1 mA/mm. For Sample B, a maximum V_{BR} 193 V was observed at $V_{\text{GS}} = -10$ V, corresponding to an F_{BR} of 3.86 MV/cm, with V_{BR} variations ranging from 150 to 193 V depending on the device position. Breakdown drain voltage of 260 V at a gate bias of -11 V was measured for Sample C (includes SiN_x passivation and the gate-connected field plate) (Supplementary Figure S1 (b)). The highest average field (F_{BR}) is therefore 5.3 MV/cm, not including the gate bias potential itself. The breakdown voltage varied between 185 V and 260 V across the wafer. To the best of our knowledge, these off-state transistor breakdown voltage values represent the current state-of-art among reported UWBG AlGaIn transistors, and are very similar to the highest breakdown field seen in another ultra-wide bandgap semiconductor [38, 39]. It is encouraging to see significantly higher breakdown field when compared with typical GaN-channel devices ($F_{\text{BR}} \sim 1\text{-}2$ MV/cm), and confirms the potential of UWBG AlGaIn for high-power RF applications [11].

At longer gate-drain distances, the breakdown voltage increased but at a slower rate, leading to lower average breakdown electric field. For example, at an $L_{\text{GD}} = 3.7 \mu\text{m}$ a breakdown voltage of 660 V was measured (Supplementary Figure S1 (b)). These excellent off-state characteristics point to the high intrinsic breakdown strength of the barrier and channel AlGaIn material, as well as the high quality of the

dielectric $\text{Al}_2\text{O}_3/\text{Al}_{0.77}\text{Ga}_{0.23}\text{N}$ interface [10]. This result supports the potential of highly scaled UWBG AlGaIn transistors for THz-frequency switching applications with enhanced breakdown performance.

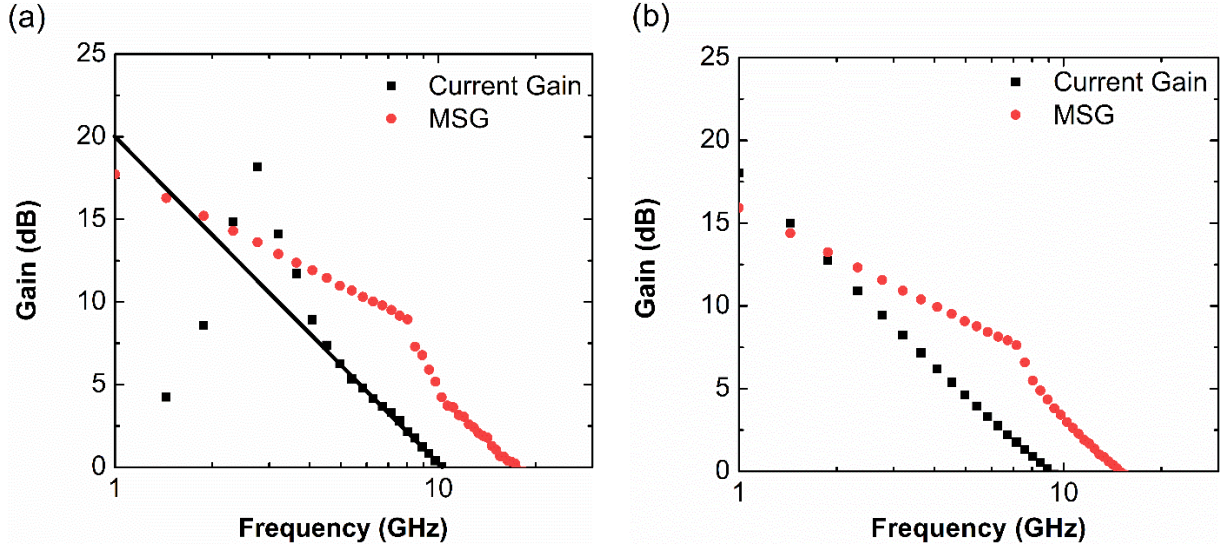


Figure 6. Small signal measurements for (a) Sample B measured at $V_{GS} = -3$ V and $V_{DS} = 13$ V, exhibiting $f_T = 10.3$ GHz, $f_{MAX} = 17.5$ GHz (b) Sample C at $V_{GS} = -2.5$ V and $V_{DS} = 10$ V, showing $f_T = 9.1$ GHz, $f_{MAX} = 15$ GHz

On-wafer small-signal measurements were performed on devices with dimensions similar to those used for on-state and off-state DC characterization. The measurements were done using Agilent vector network analyzer 8510C. The DC bias point used for Sample B was $V_{GS} = -3$ V and $V_{DS} = 13$ V, and $V_{GS} = -2.5$ V and $V_{DS} = 10$ V for Sample C. Figure 6 displays the estimated short-circuit current gain and unilateral power gain in dB scale as a function of measured frequency. Sample B had 10.3 GHz of f_T and 17.5 GHz of f_{MAX} , whereas Sample C exhibited 9.1 GHz of f_T and 15 GHz of f_{MAX} . We suspect decreased RF performances of Sample C may possibly be due to the additional parasitic capacitance components induced by the device structure and field plate with passivation. Although the RF characteristics exhibited a slight degradation due to the field-plated structure, this approach remains a viable electric field management technique, considering the significant improvements in breakdown performance

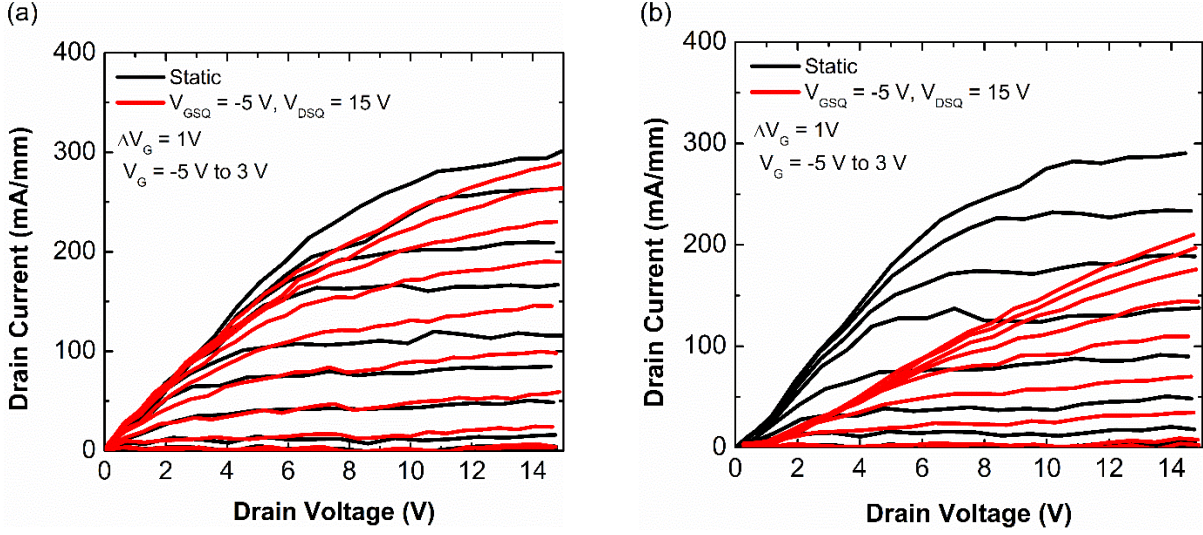


Figure 7. Pulsed I-V measurements at DC bias $V_{GS} = -5 \sim 3$ V, $V_{DS} = 0 \sim 15$ V (a) Sample B, (b) Sample C, each sample was measured using quiescent bias point of $V_{GSQ} = -5$ V, $V_{DSQ} = 15$ V with 5 μ s pulse width and 5 ms period.

To assess the trap-related characteristics, pulsed I-V measurements were conducted via DIVA D265 (Figure 7). The samples showed some current collapse and knee walkout, which may be due to a either surface and buffer trap states. A higher current collapse was observed in the passivated device (Sample C), the origin of this is not clear but could be due to unintentional variation among samples during the growth.

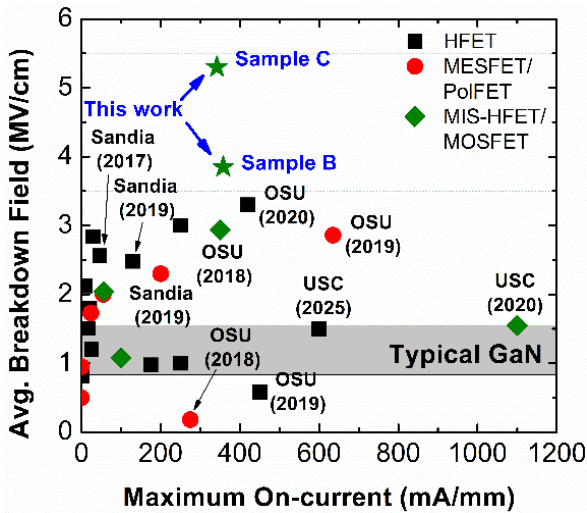


Figure 8. F_{BR} vs. I_{MAX} Benchmark plot of UWBG AlGaIn transistors [12-32]

Finally, the fabricated devices were evaluated based on F_{BR} and I_{MAX} , two key parameters for high-power RF applications, in comparison with previously reported UWBG AlGaIn transistors. Figure 8

presents the benchmark plot of F_{BR} versus I_{MAX} for UWBG AlGaIn transistors [12-32]. This benchmark analysis indicates that the transistors demonstrated in this study achieve state-of-the-art F_{BR} with excellent I_{MAX} .

In conclusion, we have successfully demonstrated UWBG AlGaIn metal-insulator HFETs with state-of-the-art average breakdown field and high maximum on-current. Utilizing a conventional field management approach incorporating passivation and a gate field plate, we achieved an average breakdown field of 5.3 MV/cm in $Al_{0.77}GaIn/Al_{0.69}GaIn$ HFET. For on-state characteristics, high maximum on-current of 358 mA/mm was realized with improved $R_{ON} = 3.26 \Omega \cdot mm$ facilitated by the implementation of a continuously grown reverse-graded ohmic contact layer. Regard RF performance, a peak f_T of 9.1 GHz and $f_{MAX} = 15$ GHz was achieved. Additionally, trap-related characteristics were assessed through pulsed I-V measurements, revealing high epitaxial quality with low gate and drain lag. These results suggest that UWBG AlGaIn transistors with optimized gate dielectrics and field management techniques hold great potential for high-power mm-wave RF applications.

This work was funded by ARO DEVCOM under Grant No. W911NF2220163 (UWBG RF Center, program manager Dr. Tom Oder). This article has been authored by an employee of National Technology & Engineering Solutions of Sandia, LLC under Contract No. DE-NA0003525 with the U.S. Department of Energy (DOE). The employee owns all right, title and interest in and to the article and is solely responsible for its contents. The United States Government retains and the publisher, by accepting the article for publication, acknowledges that the United States Government retains a non-exclusive, paid-up, irrevocable, world-wide license to publish or reproduce the published form of this article or allow others to do so, for United States Government purposes. The DOE will provide public access to these results of federally sponsored research in accordance with the DOE Public Access Plan <https://www.energy.gov/downloads/doe-public-access-plan>

Supplementary materials

In this material, we all included the breakdown results measured by varying the gate-to-drain spacings and the 2D TCAD simulation results to investigate the electric field distribution at breakdown condition for each sample.

References

- [1] M. E. Coltrin, A. G. Baca, and R. J. Kaplar, "Analysis of 2D Transport and Performance Characteristics for Lateral Power Devices Based on AlGaIn Alloys," *ECS J. Solid State Sci. Technol.*, vol. 6, no. 11, p. S3114, Oct. 2017, doi: [10.1149/2.0241711jss](https://doi.org/10.1149/2.0241711jss).

- [2] M. E. Coltrin and R. J. Kaplar, "Transport and breakdown analysis for improved figure-of-merit for AlGa_N power devices," *Journal of Applied Physics*, vol. 121, no. 5, p. 055706, Feb. 2017, doi: [10.1063/1.4975346](https://doi.org/10.1063/1.4975346).
- [3] R. J. Kaplar et al., "Review—Ultra-Wide-Bandgap AlGa_N Power Electronic Devices," *ECS J. Solid State Sci. Technol.*, vol. 6, no. 2, p. Q3061, Dec. 2016, doi: 10.1149/2.0111702jss.
- [4] A. G. Baca, A. M. Armstrong, B. A. Klein, A. A. Allerman, E. A. Douglas, and R. J. Kaplar, "Al-rich AlGa_N based transistors," *Journal of Vacuum Science & Technology A: Vacuum, Surfaces, and Films*, vol. 38, no. 2, p. 020803, Mar. 2020, doi: 10.1116/1.5129803.
- [5] T. L. Chu and R. W. Kelm, "The Preparation and Properties of Aluminum Nitride Films," *J. Electrochem. Soc.*, vol. 122, no. 7, p. 995, Jul. 1975, doi: 10.1149/1.2134385.
- [6] J. L. Hudgins, G. S. Simin, E. Santi, and M. A. Khan, "An assessment of wide bandgap semiconductors for power devices," *IEEE Transactions on Power Electronics*, vol. 18, no. 3, pp. 907–914, May 2003, doi: 10.1109/TPEL.2003.810840.
- [7] Zhu, Y., Allerman, A. A., Joishi, C., Pratt, J., Dominic Merwin Xavier, A. M., Calderon Ortiz, G., Klein, B. A., Armstrong, A., Hwang, J., & Rajan, S. (2025). Heterostructure and interfacial engineering for low-resistance contacts to ultra-wide bandgap AlGa_N. *Applied Physics Letters*, 126(6), 062107. <https://doi.org/10.1063/5.0230220>
- [8] Alam, M. T., Chen, J., Stephenson, K., Mamun, M. A.-A., Mazumder, A. A. M., Pasayat, S. S., Khan, A., & Gupta, C. (2025). 2 kV Al_{0.64}Ga_{0.36}N-channel high electron mobility transistors with passivation and field plates. *Applied Physics Express*, 18(1), 016504. <https://doi.org/10.35848/1882-0786/ad9db4>
- [9] Chen, J., Seshadri, P., Stephenson, K., Mamun, M. A., Bai, R., Wang, Z., Khan, A., & Gupta, C. (2025). 64% AlGa_N channel HFET with high Johnson's Figure of Merit (> 6THz·V). *IEEE Electron Device Letters*, 1–1. *IEEE Electron Device Letters*. <https://doi.org/10.1109/LED.2025.3541145>
- [10] Shin, S., Liddy, K., Zhu, Y., Joishi, C., Klein, B. A., Armstrong, A., Allerman, A. A., & Rajan, S. (2025). Energy Bands and Breakdown Characteristics in Al₂O₃/UWBG AlGa_N Heterostructures (arXiv:2504.01291). arXiv. <https://doi.org/10.48550/arXiv.2504.01291>
- [11] Çiçek, O., & Badali, Y. (2024). A Review: Breakdown Voltage Enhancement of Ga_N Semiconductors-Based High Electron Mobility Transistors. *IEEE Transactions on Device and Materials Reliability*, 24(2), 275–286. *IEEE Transactions on Device and Materials Reliability*. <https://doi.org/10.1109/TDMR.2024.3379745>
- [12] Tokuda, H., Hatano, M., Yafune, N., Hashimoto, S., Akita, K., Yamamoto, Y., & Kuzuhara, M. (2010). High Al Composition AlGa_N-Channel High-Electron-Mobility Transistor on AlN Substrate. *Applied Physics Express*, 3(12), 121003
- [13] Okumura, H., Suihkonen, S., Lemettinen, J., Uedono, A., Zhang, Y., Piedra, D., & Palacios, T. (2018). AlN metal–semiconductor field-effect transistors using Si-ion implantation. *Japanese Journal of Applied Physics*, 57(4S), 04FR11. <https://doi.org/10.7567/JJAP.57.04FR11>
- [14] Xue, H., Lee, C. H., Hussian, K., Razzak, T., Abdullah, M., Xia, Z., Soheli, S. H., Khan, A., Rajan, S., & Lu, W. (2019). Al_{0.75}Ga_{0.25}N/Al_{0.6}Ga_{0.4}N heterojunction field effect transistor with f_T of 40 GHz. *Applied Physics Express*, 12(6), 066502. <https://doi.org/10.7567/1882-0786/ab1cf9>
- [15] Muhtadi, S., Hwang, S. M., Coleman, A., Asif, F., Simin, G., Chandrashekhar, M., & Khan, A. (2017). High Electron Mobility Transistors With Al_{0.65}Ga_{0.35}N Channel Layers on Thick AlN/Sapphire Templates. *IEEE Electron Device Letters*, 38(7), 914–917. *IEEE Electron Device Letters*. <https://doi.org/10.1109/LED.2017.2701651>
- [16] Bajaj, S., Allerman, A., Armstrong, A., Razzak, T., Talesara, V., Sun, W., Soheli, S. H., Zhang, Y., Lu, W., Arehart, A. R., Akyol, F., & Rajan, S. (2018). High Al-Content AlGa_N Transistor With 0.5 A/mm Current Density and Lateral Breakdown Field Exceeding 3.6 MV/cm. *IEEE Electron Device*

- Letters*, 39(2), 256–259. IEEE Electron Device Letters. <https://doi.org/10.1109/LED.2017.2780221>
- [17] Armstrong, A. M., Klein, B. A., Baca, A. G., Allerman, A. A., Douglas, E. A., Colon, A., Abate, V. M., & Fortune, T. R. (2019). AlGa_N polarization-doped field effect transistor with compositionally graded channel from Al_{0.6}Ga_{0.4}N to AlN. *Applied Physics Letters*, 114(5), 052103. <https://doi.org/10.1063/1.5058263>
- [18] Baca, A. G., Klein, B. A., Wendt, J. R., Lepkowski, S. M., Nordquist, C. D., Armstrong, A. M., Allerman, A. A., Douglas, E. A., & Kaplar, R. J. (2019). RF Performance of Al_{0.85}Ga_{0.15}N/Al_{0.70}Ga_{0.30}N High Electron Mobility Transistors With 80-nm Gates. *IEEE Electron Device Letters*, 40(1), 17–20. IEEE Electron Device Letters. <https://doi.org/10.1109/LED.2018.2880429>
- [19] Baca, A. G., Klein, B. A., Allerman, A. A., Armstrong, A. M., Douglas, E. A., Stephenson, C. A., Fortune, T. R., & Kaplar, R. J. (2017). Al_{0.85}Ga_{0.15}N/Al_{0.70}Ga_{0.30}N High Electron Mobility Transistors with Schottky Gates and Large On/Off Current Ratio over Temperature. *ECS Journal of Solid State Science and Technology*, 6(12), Q161. <https://doi.org/10.1149/2.0231712jss>
- [20] Bajaj, S., Akyol, F., Krishnamoorthy, S., Zhang, Y., & Rajan, S. (2016). AlGa_N channel field effect transistors with graded heterostructure ohmic contacts. *Applied Physics Letters*, 109(13), 133508. <https://doi.org/10.1063/1.4963860>
- [21] Singhal, J., Kim, E., Hickman, A., Chaudhuri, R., Cho, Y., Xing, H. G., & Jena, D. (2023). AlN/AlGa_N/AlN quantum well channel HEMTs. *Applied Physics Letters*, 122(22), 222106. <https://doi.org/10.1063/5.0145582> M. E. Coltrin and R. J. Kaplar, “Transport and breakdown analysis for improved figure-of-merit for AlGa_N power devices,” *Journal of Applied Physics*, vol. 121, no. 5, p. 055706, Feb. 2017, doi: [10.1063/1.4975346](https://doi.org/10.1063/1.4975346).
- [22] Gaevski, M., Mollah, S., Hussain, K., Letton, J., Mamun, A., Jewel, M. U., Chandrashekhar, M., Simin, G., & Khan, A. (2020). Ultrawide bandgap Al_xGa_{1-x}N channel heterostructure field transistors with drain currents exceeding 1.3 A mm⁻¹. *Applied Physics Express*, 13(9), 094002. <https://doi.org/10.35848/1882-0786/abb1c8>
- [23] Razzak, T., Hwang, S., Coleman, A., Bajaj, S., Xue, H., Zhang, Y., Jamal-Eddine, Z., Sohel, S. h., Lu, W., Khan, A., & Rajan, S. (2018). RF operation in graded AlGa_{1-x}N (x = 0.65 to 0.82) channel transistors. *Electronics Letters*, 54(23), 1351–1353. <https://doi.org/10.1049/el.2018.6897>
- [24] Armstrong, A. M., Klein, B. A., Colon, A., Allerman, A. A., Douglas, E. A., Baca, A. G., Fortune, T. R., Abate, V. M., Bajaj, S., & Rajan, S. (2018). Ultra-wide band gap AlGa_N polarization-doped field effect transistor. *Japanese Journal of Applied Physics*, 57(7), 074103. <https://doi.org/10.7567/JJAP.57.074103>
- [25] Khachariya, D., Mita, S., Reddy, P., Dangi, S., Dycus, J. H., Bagheri, P., Breckenridge, M. H., Sengupta, R., Rathkanthiwar, S., Kirste, R., Kohn, E., Sitar, Z., Collazo, R., & Pavlidis, S. (2022). Record >10 MV/cm mesa breakdown fields in Al_{0.85}Ga_{0.15}N/Al_{0.6}Ga_{0.4}N high electron mobility transistors on native AlN substrates. *Applied Physics Letters*, 120(17), 172106. <https://doi.org/10.1063/5.0083966>
- [26] Da, B., Herath Mudiyanse, D., Wang, D., He, Z., & Fu, H. (2024). High-voltage kV-class AlN metal-semiconductor field-effect transistors on single-crystal AlN substrates. *Applied Physics Express*, 17(10), 104002. <https://doi.org/10.35848/1882-0786/ad85c0>
- [27] Alam, M. T., Chen, J., Stephenson, K., Mamun, M. A.-A., Mazumder, A. A. M., Pasayat, S. S., Khan, A., & Gupta, C. (2025). 2 kV Al_{0.64}Ga_{0.36}N-channel high electron mobility transistors with passivation and field plates. *Applied Physics Express*, 18(1), 016504. <https://doi.org/10.35848/1882-0786/ad9db4>
- [28] Kometani, Y., Kawaide, T., Tanaka, S., Egawa, T., & Miyoshi, M. (2024). AlN/AlGa_N heterojunction field-effect transistors with a high-AlN-mole-fraction Al_{0.72}Ga_{0.28}N channel grown on single-

- crystal AlN substrate by metalorganic chemical vapor deposition. Japanese Journal of Applied Physics, 63(11), 111003. <https://doi.org/10.35848/1347-4065/ad85ed>
- [29] Abid, I., Mehta, J., Cordier, Y., Derluyn, J., Degroote, S., Miyake, H., & Medjdoub, F. (2021). AlGa_N Channel High Electron Mobility Transistors with Regrown Ohmic Contacts. Electronics, 10(6), Article 6. <https://doi.org/10.3390/electronics10060635>
- [30] Baca, A. G., Armstrong, A. M., Allerman, A. A., Douglas, E. A., Sanchez, C. A., King, M. P., Coltrin, M. E., Fortune, T. R., & Kaplar, R. J. (2016). An AlN/Al_{0.85}Ga_{0.15}N high electron mobility transistor. Applied Physics Letters, 109(3), 033509. <https://doi.org/10.1063/1.4959179>
- [31] Maeda, R., Ueno, K., Kobayashi, A., & Fujioka, H. (2022). AlN/Al_{0.5}Ga_{0.5}N HEMTs with heavily Si-doped degenerate GaN contacts prepared via pulsed sputtering. Applied Physics Express, 15(3), 031002. <https://doi.org/10.35848/1882-0786/ac4fcf>
- [32] Chen, J., Seshadri, P., Stephenson, K., Mamun, M. A., Bai, R., Wang, Z., Khan, A., & Gupta, C. (2025). 64% AlGa_N channel HFET with high Johnson's Figure of Merit (> 6THz·V). IEEE Electron Device Letters, 1–1. IEEE Electron Device Letters. <https://doi.org/10.1109/LED.2025.3541145>
- [33] Maeda, R., Ueno, K., Kobayashi, A., and Fujioka, H. (2022). AlN/Al_{0.5}Ga_{0.5}N HEMTs with heavily Si-doped degenerate GaN contacts prepared via pulsed sputtering. Applied Physics Express, 15 031002. <https://doi.org/10.35848/1882-0786/ac4fcf>
- [34] Xue, H., Hussain, K., Razzak, T., Gaevski, M., Soheli, S. H., Mollah, S., Talesara, V., Khan, A., Rajan, S., Lu, W. (2020) Al_{0.65}Ga_{0.35}N/Al_{0.4}Ga_{0.6}N Micro-Channel Heterojunction Field Effect Transistors With Current Density Over 900 mA/mm. IEEE Electron Device Letters, 41-5. <https://doi.org/10.1109/LED.2020.2977997>
- [35] Zhang, Z., Jackson, C. M., Arehart, A. R., McSkimming, B., Speck, J. S., & Ringel, S. A. (2014). Direct Determination of Energy Band Alignments of Ni/Al₂O₃/Ga_N MOS Structures Using Internal Photoemission Spectroscopy. Journal of Electronic Materials, 43(4), 828–832. <https://doi.org/10.1007/s11664-013-2942-z>
- [36] Di Lecce, V., Krishnamoorthy, S., Esposto, M., Hung, T.-H., Chini, A., & Rajan, S. (2012). Metal-oxide barrier extraction by Fowler-Nordheim tunnelling onset in Al₂O₃-on-GaN MOS diodes. Electronics Letters, 48(6), 347–348. <https://doi.org/10.1049/el.2011.4046>
- [37] SILVACO, Inc., 2021 Atlas User's Manual (SILVACO, Inc., Santa Clara, CA, 2021).
- [38] Kalarickal, N. K., Xia, Z., Huang, H.-L., Moore, W., Liu, Y., Brenner, M., Hwang, J., & Rajan, S. (2021). β-(Al_{0.18}Ga_{0.82})₂O₃/Ga₂O₃ Double Heterojunction Transistor With Average Field of 5.5 MV/cm. IEEE Electron Device Letters, 42(6), 899–902. <https://doi.org/10.1109/LED.2021.3072052>
- [39] Dhara, S., Kalarickal, N. K., Dheenani, A., Joishi, C., & Rajan, S. (2022). β-Ga₂O₃ Schottky barrier diodes with 4.1 MV/cm field strength by deep plasma etching field-termination. Applied Physics Letters, 121(20), 203501. <https://doi.org/10.1063/5.0123284>

Supplementary Information

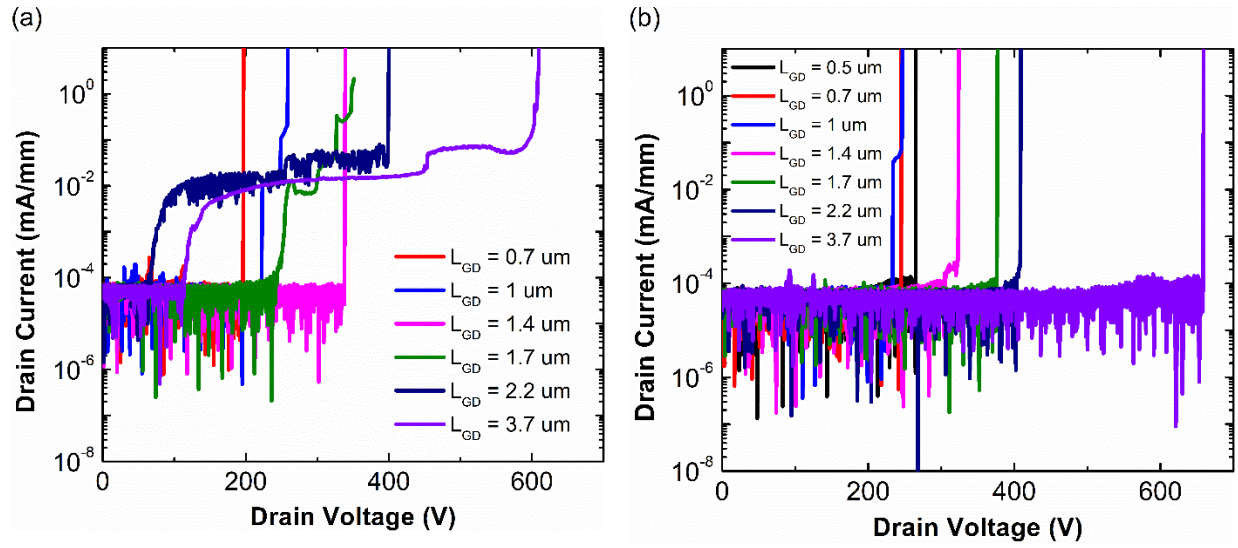


Figure S1. Three-terminal breakdown measurements of (a) Sample B varying $L_{GD} = 0.7 \sim 3.7 \mu\text{m}$, (b) Sample C varying $L_{GD} = 0.5 \sim 3.7 \mu\text{m}$

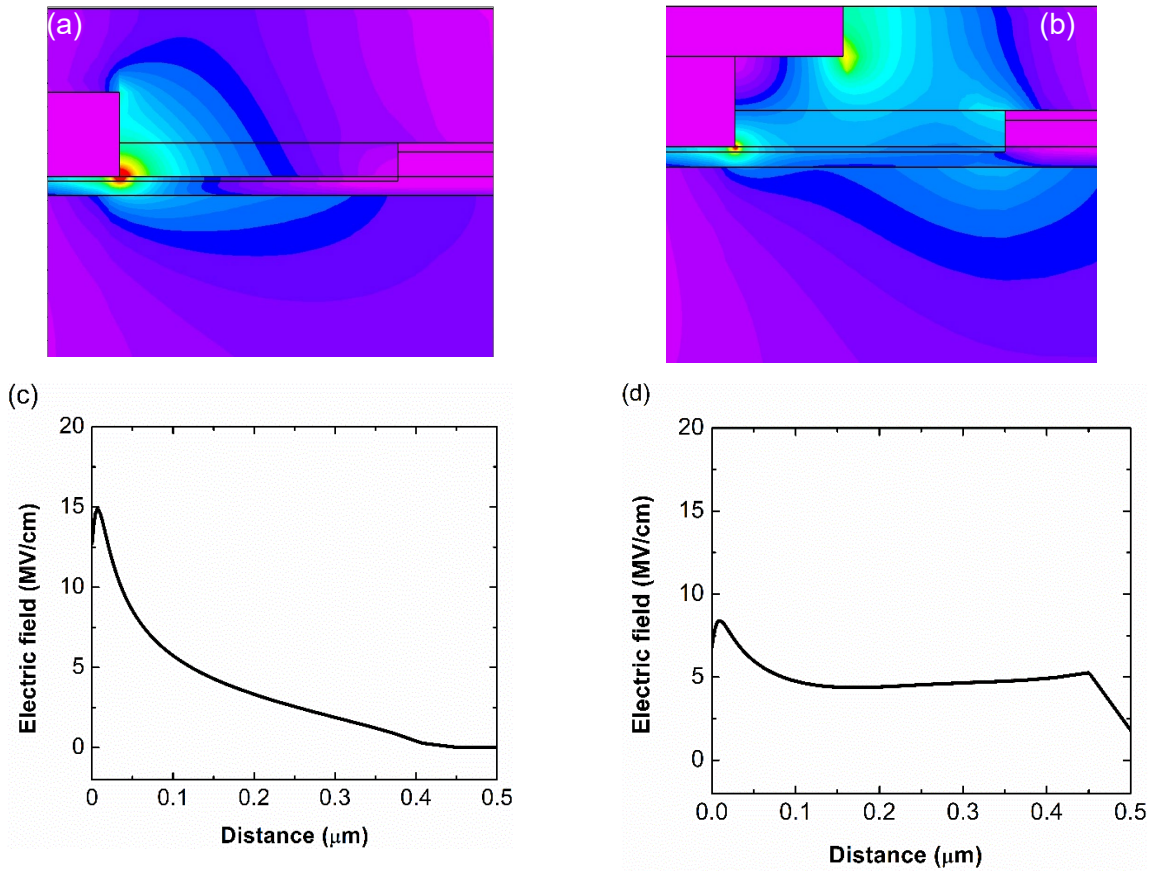


Figure S2. (a) Simulated electric field distribution of Sample B at $V_{GS} = -10$ V and $V_{DS} = 193$ V, (b) simulated electric field distribution of Sample C at $V_{GS} = -11$ V and $V_{DS} = 260$ V, (c) x-direction electric field profile of Sample B, cutline at $Al_2O_3/AlGaN$ barrier interface, (d) x-direction electric field profile of Sample C, cutline at $Al_2O_3/AlGaN$ barrier interface

Three-terminal breakdown measurements with varying gate-to-drain spacing are shown in Figure S1(a), (b). Some devices from Sample B show increasing leakage current with V_{DS} , Sample C devices (with SiN_x passivation and field plates) showed almost constant leakage for all L_{GD} values until the device undergoes “hard” and irreversible breakdown. Further investigation is needed to understand the exact breakdown mechanisms, but we did breakdown simulations were performed using 2D TCAD modeling [37]. From the simulation results, the x-direction peak electric field ($E_{X,PEAK}$) was evaluated as 14.8 MV/cm for Sample B under breakdown condition, while Sample C showed a significantly lower $E_{X,PEAK}$ of 8.39 MV/cm at $V_{DS} = 260$ V. Furthermore, it was found that field-plated devices (Sample C) exhibited a more uniform, box-like electric field profile compared to non-field-plated structures (Sample B), which displayed a non-uniform field distribution. The effective peak electric field (F_{eff}) was calculated using $F_{OX} = 1.54$ MV/cm, as determined in our previous dielectric study, yielding values of 14.88 MV/cm for Sample B and 8.53 MV/cm for Sample C [10]. These simulation results suggest that SiN_x passivation and field plating—when applied under the same passivation thickness and field plate length conditions as the fabricated devices—can effectively reduce the peak electric field and promote a more uniform electric field distribution, thereby enabling higher voltage handling within the same device dimensions.

Differences in the leakage characteristics among devices in sample B may be due to variations in epitaxial structure, or in the process conditions/exact geometry of the gate (e.g. the real gate profile may not be a right angle as assumed in the simulation).